AIAA JOURNAL
Vol. 32, No. 9, September 1994

Vortical and Turbulent Structure of a Lobed Mixer Free Shear Layer

D. C. McCormick*
United Technologies Research Center, East Hartford, Connecticut 06108
and
J. C. Bennett Jr.†
University of Connecticut, Storrs, Connecticut 06268

An experimental investigation of the vortical and turbulent structure in a free shear layer downstream of a lobed mixer has been conducted. Pulsed-laser sheet flow visualization with smoke and three-dimensional velocity measurements with hot-film anemometry were obtained for a lobed-mixer configuration and a baseline, planar configuration. Laminar and turbulent initial boundary-layer conditions were documented for both cases. The main result of this investigation is that a new vortex structure was confirmed to exist for the lobed mixer in addition to the well-known streamwise vortex array, consistent with the work of Manning. The normal vortex (due to the Kelvin-Helmholtz instability) sheds periodically from the convoluted trailing edge of the lobed mixer and plays a major part in the enhanced mixing process in combination with the streamwise vorticity. The streamwise vorticity deforms the normal vortex into a pinched-off structure that is unstable and creates intense small-scale turbulence and mixing.

Nomenclature

f_{kh} = frequency of the Kelvin-Helmholtz instability
H = lobe height
k = turbulent kinetic energy, $(\overline{u^2} + \overline{v^2} + \overline{w^2})/2$
Re_θ = boundary-layer Reynolds number, $U_i\theta_i/\nu$, $i = 1, 2$
St_θ = Strouhal number, $f_{kh}\theta_1/\overline{U}$
U = mean axial velocity component
$\overline{U}$ = average stream velocity, $(U_1 + U_2)/2$
U_1 = high-speed velocity
U_2 = low-speed velocity
u = fluctuating axial velocity component
V = mean vertical velocity component
v = fluctuating vertical velocity component
W = mean spanwise velocity component or lobe width
w = fluctuating spanwise velocity component
x = axial coordinate
y = vertical coordinate
z = spanwise coordinate
ΔU = freestream velocity difference, U_1-U_2
δ_i = boundary-layer thickness upstream of trailing edge, $i = 1, 2$
δ_i^* = displacement thickness upstream of trailing edge, $i = 1, 2$
θ = shear layer momentum thickness, Eq. (2)
θ_i = momentum thickness upstream of trailing edge, $i = 1, 2$
λ_{kh} = wavelength of the Kelvin-Helmholtz instability
ω_x = streamwise vorticity

Introduction

THE lobed mixer is an extraordinary fluid mechanic device for efficiently mixing two coflowing streams of different velocities, temperatures, and/or species. The lobed mixer consists of a splitter plate with a convoluted trailing edge, as shown in Fig. 1, which alternately turns the upper and lower streams into the lobe troughs. As illustrated in the exit plane view in Fig. 1, this flow turning creates a shear layer in the cross-stream plane along the vertical edges of the lobed mixer. Previous research has shown this distributed streamwise vorticity develops into an array of counter-rotating vortices which are believed to be primarily responsible for the enhanced mixing. However, the detailed mechanisms by which the lobed mixer substantially enhances the mixing of the two streams relative to a straight splitter plate (planar free shear layer) remains largely undefined.

The first application of the lobed mixer was for jet noise reduction of a turbofan jet engine.[1] The high-velocity core flow was mixed with the lower velocity fan flow using a lobed mixer, thereby reducing the peak exit velocity and thus substantially reducing jet noise [jet noise ~ $(U_{peak})^8$]. This application was even more successful in that, for the first time, a jet noise reduction strategy also resulted in a net thrust increase. The thrust augmentation associated with the heat transfer from the low-loss mixing process, resulted in the lobed-mixer concept being a significant part of the NASA sponsored Energy Efficient Engine program ini-

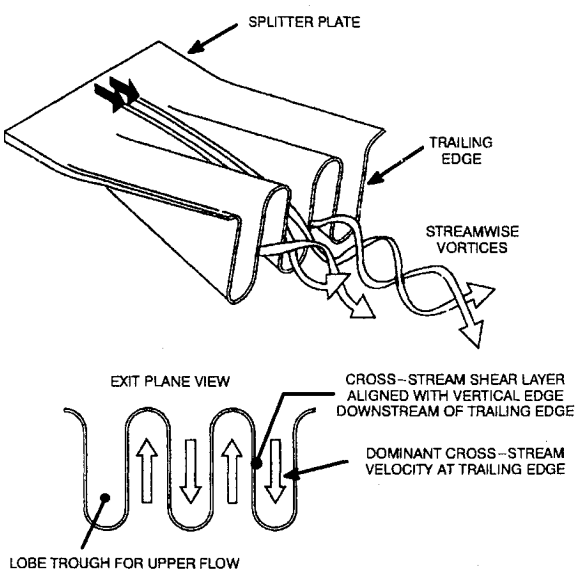

Fig. 1 Lobed-mixer concept.

Presented as Paper 93-0219 at the AIAA 31st Aerospace Sciences Meeting, Reno, NV, Jan. 11–14, 1993; received March 23, 1993; revision received Feb. 25, 1994; accepted for publication March 15, 1994.

*Senior Research Engineer, Aeroacoustics and Experimental Gas Dynamics Section, 411 Silver Lane. Member AIAA.
†Associate Professor, Department of Mechanical Engineering.

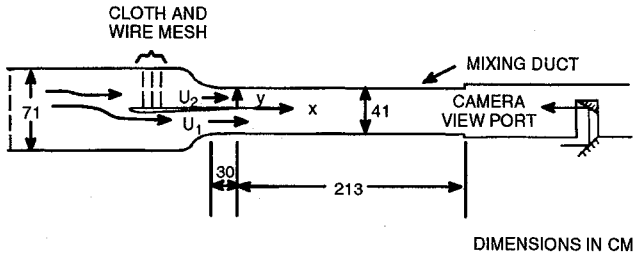

Fig. 2 Schematic of test section.

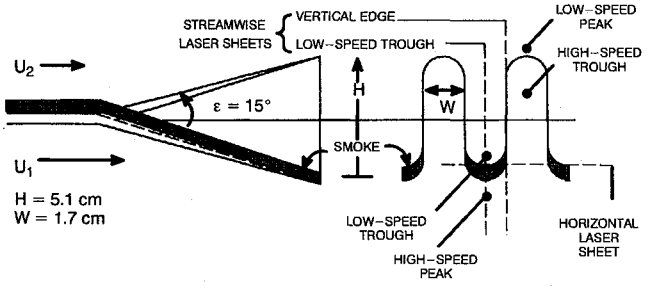

Fig. 3 Lobed mixer and nomenclature.

tiated in 1978.[2] Since then, the lobed mixer has also become an integral design feature of ejector applications.[3] The so-called mixer-ejector concept is under consideration for noise reduction on the high-speed civil transport[4] and has been successfully integrated into a retrofit noise reduction kit, enabling older jet engines to meet federal noise regulations.[5]

Originally, it was believed that the mixing enhancement mechanism was solely due to the increased interfacial area.[6] However, subsequent studies by Paterson[7] and Povinelli et al.[8] under the Energy Efficient Engine program revealed that the flowfield was dominated by secondary flow structures (large-scale, streamwise vorticity, Fig. 1), which played a major role in the enhanced mixing process. More recently, it has become obvious that lobed mixers provide the most mixing enhancement in the presence of a velocity difference or normal vorticity component. The work of Manning[9] (recently summarized by Elliott et al.[10]), clearly showed that the mixing enhancement of the lobed mixer increased with increasing velocity ratio between the streams. In hindsight, the success of the turbofan engine and the mixer-ejector applications is rooted in the inherent velocity ratio that is present in both cases. Thus, it is important that the free shear flowfield downstream of a lobed mixer be thoroughly comprehended for complete exploitation of the mixing technology.

The purpose of this investigation is to provide this fundamental understanding of the vortical and turbulent structure of a lobed mixer free shear layer to enable realistic flow modeling of the mixing process and to provide an understanding of why mixing effectiveness of lobed mixers varies with application. The approach selected for the present investigation is a low-speed wind-tunnel experiment in which instantaneous flow visualization and three-dimensional velocity measurements were obtained. For both a lobed-mixer case and a baseline planar case, laminar and turbulent initial boundary layers were investigated. Though the turbulent initial condition is more practical, the laminar initial condition was also studied since turbulent initial conditions can mask the flow structure and bypass certain instabilities.

Surprisingly, there are only a few fundamental, detailed experimental free shear layer studies known to exist for lobed mixers. Of these studies, the most significant for understanding flow structure and turbulence characteristics are by Manning[9] and Eckerle et al.[11] Eckerle reported detailed three-dimensional laser Doppler velocimetry measurements for a lobed mixer but did not provide corresponding flow visualization nor baseline, planar results. Manning investigated the molecular mixing of three configurations, a straight splitter plate (planar case), a lobed mixer, and a convoluted plate (same exit waveform as the lobed mixer, but no streamwise vorticity), which clarified the role of the streamwise vorticity and the increased interfacial area on the enhanced mixing. The major conclusions were that the convoluted plate provided about half the mixing augmentation of the lobed mixer and, more importantly, the mixing augmentation of the lobed mixer relative to the convoluted plate increased with velocity ratio. Manning also observed a new vortex structure periodically shed from the lobed mixer associated with the Kelvin-Helmholtz instability. However, detailed flowfield measurements were not obtained and the free shear layer was significantly influenced by the duct walls. Also, both studies (Refs. 9 and 11) were limited in the axial development length (~$6H$). Therefore, it is believed that the current investigation represents the most comprehensive examination of the subject flowfield. Note that the complete Reynolds stress tensor, which was documented in this study, is fully reported in Ref. 12.

Experimental Arrangement

The experiment was conducted in a closed-circuit wind tunnel. The facility's design is described by Blair et al.[13] for the development of fundamental laminar and turbulent boundary-layer studies. In the current investigation, the boundary-layer test section was replaced with a free shear layer test section with a 41-cm × 41-cm cross section, which is shown in Fig. 2. Figure 2 also gives the coordinate system for the present investigation: x axial, y lateral or vertical, and z spanwise or out of the paper.

The velocity difference across the free shear layer was created by dividing the flow with a splitter plate that had flow resistance on one side. The plate's leading edge was cambered, and suction was applied to control the overspeed separation on the lower surface and maintain laminar boundary layers. The highest obtainable velocity ratio with laminar boundary layers was $U_1/U_2 = 1.75$, the test condition for the current investigation. The splitter plate was tapered at a 2.2-deg included angle to the knife-edged trailing edge (0.25-mm trailing-edge radius). The splitter plate extended 30 cm into the 41-cm × 41-cm mixing duct test section to insure uniformly straight flow at the trailing edge. The axial length of the mixing duct was 2.44 m (2.13 m downstream of the trailing edge). The top and bottom walls were instrumented with static pressure taps that were used to adjust the side walls to provide a zero pressure gradient. The side walls were diverged 6.4 mm over 2.44 m (0.15 deg) to achieve zero gradient conditions.

Figure 3 gives a schematic diagram of the lobed mixer design. As seen in the figure, the waveform of the lobed mixer was symmetric with vertical lobe walls and circular troughs. The lobe aspect ratio was $H/W = 3.0$ (lobe height $H = 5.1$ cm), and the trough angle was $\varepsilon = 15$ deg. This design is relatively conservative (that is, moderate trough angle and aspect ratio) and is similar to the symmetric geometries studied by Manning[9] and Eckerle et al.[11]

Initial Boundary Layers

The initial boundary layers were measured 2.54 cm upstream of the splitter-plate trailing edge ($x = -2.54$ cm) with a single sensor hot-film probe. Surveys of velocity were obtained at $z = 0$, 10.2, and −10.2 cm (0, 25%, and −25% span) on the high- and low-

Table 1 Initial laminar boundary-layer conditions

Stream	U, m/s	δ, mm	δ^*, mm	θ, mm	δ^*/θ	Re_θ
1	8.53	5.3	1.27	0.589	2.163	327
2	4.88	6.4	1.69	0.724	2.338	230

Table 2 Initial turbulent boundary-layer conditions

Stream	U	δ	δ^*	θ	δ^*/θ	Re_θ
1	8.53	11.4	1.59	1.107	1.438	617
2	4.88	11.9	1.88	1.237	1.524	392

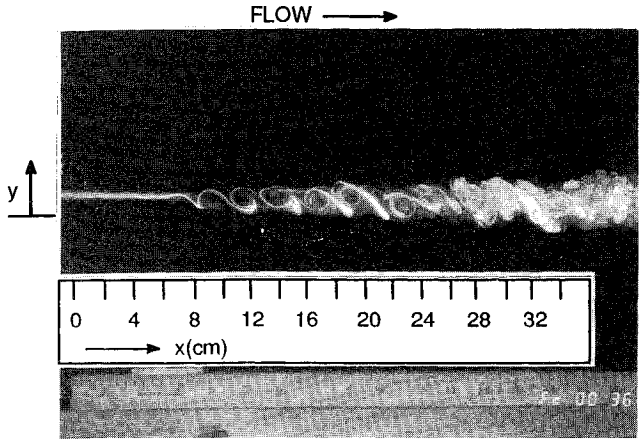

Fig. 4 Streamwise laser sheet of planar free shear layer.

speed sides of the splitter plate. Both laminar and turbulent boundary-layer conditions were documented and were found to compare well with the Blasius profile and turbulent wall region scaling, respectively. Also, the flow was found to be very two dimensional for all cases (see Ref. 12 for full details and profile plots).

Laminar Boundary Layers

The laminar boundary-layer characteristics in terms of boundary-layer thickness ($0.995U_\infty$ criterion), displacement thickness, momentum thickness, and shape factor are given in Table 1. The values listed are for the average of the three spanwise surveys. Also given in the table are the corresponding freestream velocities.

As seen in the table, the boundary-layer thickness on the low-speed side was 20% thicker due to the lower Reynolds number, despite the shorter development length. The shape factors for both sides were reasonably close to that of the Blasius profile (δ^*/θ = 2.59). The momentum thickness Reynolds number for both sides indicates that perturbations are likely to amplify and not damp out [$Re_\theta > 200$ (Ref. 14)].

Turbulent Boundary Layers

The boundary layers were tripped turbulent on both sides of the splitter plate with Hama-type trips[15] (serrated leading-edge trip) at 40 cm upstream of the trailing edge. The trips were made of vinyl strips that were cut and sanded to the desired thickness. The trip thicknesses were 1.24 and 0.97 mm on the low- and high-speed sides, respectively. The trip thickness and axial locations were found by trial and error, selected to obtain the smallest possible trip that was at least several hundred trip thicknesses upstream of the trailing edge. Table 2 gives the averaged boundary-layer parameters for the turbulent boundary layers.

The shape factor values indicate that the boundary layers are fully developed turbulent profiles ($\delta^*/\theta \approx 1.4$). The profiles in law-of-the-wall coordinates (see Ref. 12) all displayed a buffer region, a log-linear region and a wake region, indicating equilibrium boundary-layer development.

Triple-Sensor Hot-Film Probe

The triple-sensor hot-film probe was the main diagnostic tool of the investigation. The probe, a Thermal Systems Incorporated Model 1299-18-20, is a compact orthogonal arrangement which provided a spatial resolution of 2.0 mm and a large acceptance cone of 35-deg polar angle. It allowed instantaneous realization of the velocity vector and, thus, the entire Reynolds stress tensor could be obtained. For brevity in this paper, only the turbulent kinetic energy (sum of normal components of the tensor) is reported. The Reynolds shear components are discussed in Ref. 12 in detail.

The calibration method used in this investigation was a direct curve fit of the probe response over the entire range of pitch and yaw angles and velocity to a 10 coefficient polynomial curve (so-called black box method). It does not assume a cosine or Jorgensen cooling law response that requires somewhat complex solution algorithms.[16] Other advantages of this approach are probe interference effects, wake effects, h and k variations (cooling law constants), etc. are taken into account; wire sensor angles need not be accurately determined; and unique solutions are readily obtained. Note, the orthogonality of the TSI 1299 probe is not a requirement for use of this method. The disadvantage of this method is the large calibration matrix required (usually several hundred points); thus the method necessitates an automated calibration facility.

The accuracy of the calibration was evaluated to be within ±1 deg in pitch and yaw flow angles and ±1.0% in velocity magnitude. This uncertainty does not include precision error which depends on the local turbulence intensity. Each measurement consisted of 1000 independent realizations of the velocity vector. The worst case precision error (associated with the highest turbulence levels) was $\pm 0.020\Delta U$ in the mean velocity (U, V, and W) measurements (95% confidence level). The corresponding precision error for the variance measurements was calculated to be $\pm 0.009\Delta U^2$ and for the turbulent kinetic energy $\pm 0.014\Delta U^2$. In addition, a significant bias error occurs in highly turbulent flow when the instantaneous flow is outside of the probe acceptance core (35 deg). These measurements were easily identified since they would not converge in the solution algorithm and hence were rejected. This situation occurred in a substantial number of realizations (up to 20%) at some points in the first measurement plane downstream of the mixer due to the intense vortex structures. Hence, the peak turbulence measurements in this plane are biased low. This error was eliminated in the mean measurements by averaging voltages prior to entering the solution algorithm.

Flow Visualization

Flow visualization of the shear layer interfacial region was accomplished by tangential slot injection of smoke on the low-speed side of the splitter plate, upstream of the two screens (downstream

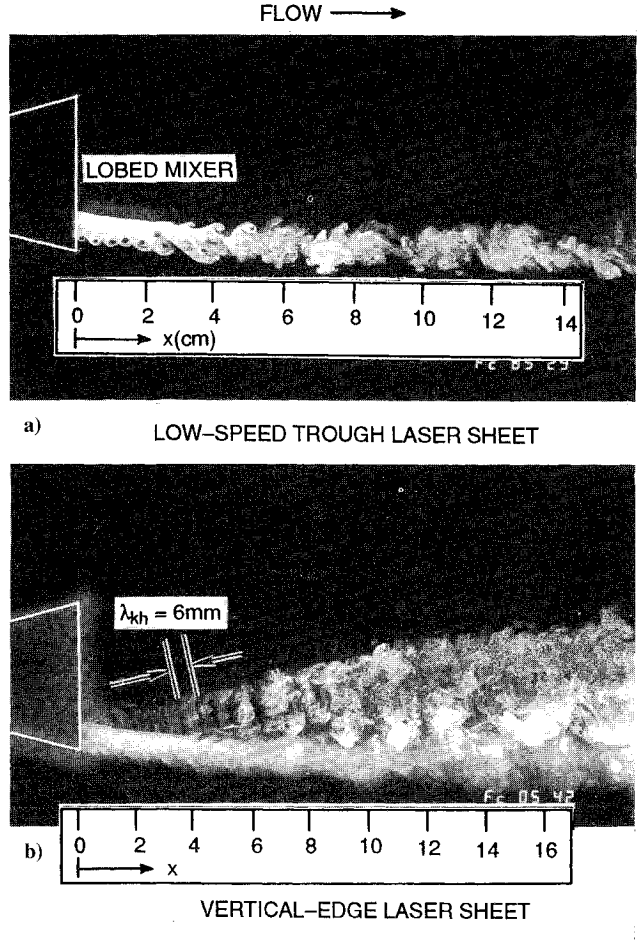

Fig. 5 Streamwise laser sheet of lobed mixer free shear layer.

of the cloth mesh). In this way, the perturbations caused by the smoke injection were minimized and laminar boundary-layer conditions could be maintained. The injection slot spanned the center 50% of the plate (20.3 cm long) and was 1 mm wide. The smoke was generated with a theatrical smoke machine (Rosco Model 1500), which atomized an alcohol-based fluid with a heater element. A Nd:YAG pulsed laser with a frequency doubler was used to generate a high-power, short-duration (10 ns) laser sheet (λ = 532 nm). Laser sheet orientations are given in Fig. 3.

Planar Free Shear Layer

Figure 4 shows the smoke flow visualization with a streamwise laser sheet (xy plane) for the laminar free shear layer. The visualization clearly shows the well-known laminar rollup of the spanwise vortices due to the Kelvin-Helmholtz instability (that is, an inflection point in mean axial velocity profile that is inviscidly unstable[17]). The initial wavelength appears to be about λ_{kh} = 2.5 cm. At about x = 24 cm, smaller scales are observed to appear indicating the onset of transition to turbulence. By x = 28 cm, the flow is fully turbulent. Vortex pairing is observed to begin near x = 20 cm. Cross-stream and horizontal laser sheet orientations are reported in Ref. 12 which clearly show the development of the streamwise instability/vorticity, consistent with the free shear layer development described by Lasheras.[18] Based on the measured Kelvin-Helmholtz frequency (f_{kh} = 270 Hz, from hot-film autospectra) of the spanwise vortices and the measured initial boundary-layer thickness, the Strouhal number was found to be St_θ = 0.024. This value is close to the experimentally determined value of St_θ = 0.030 reported by Ho and Huang.[19]

In summary, well-behaved laminar and turbulent planar free shear layers were visualized and documented for comparison with the lobed-mixer case. The velocity measurement results for growth rates and turbulence statistics and the flow visualization were found to be in good agreement with previously published results and current free shear layer understanding (see Ref. 12 for details of the comparisons to the published literature). Presentation of the shear layer growth for laminar and turbulent conditions is given later with the lobed-mixer results.

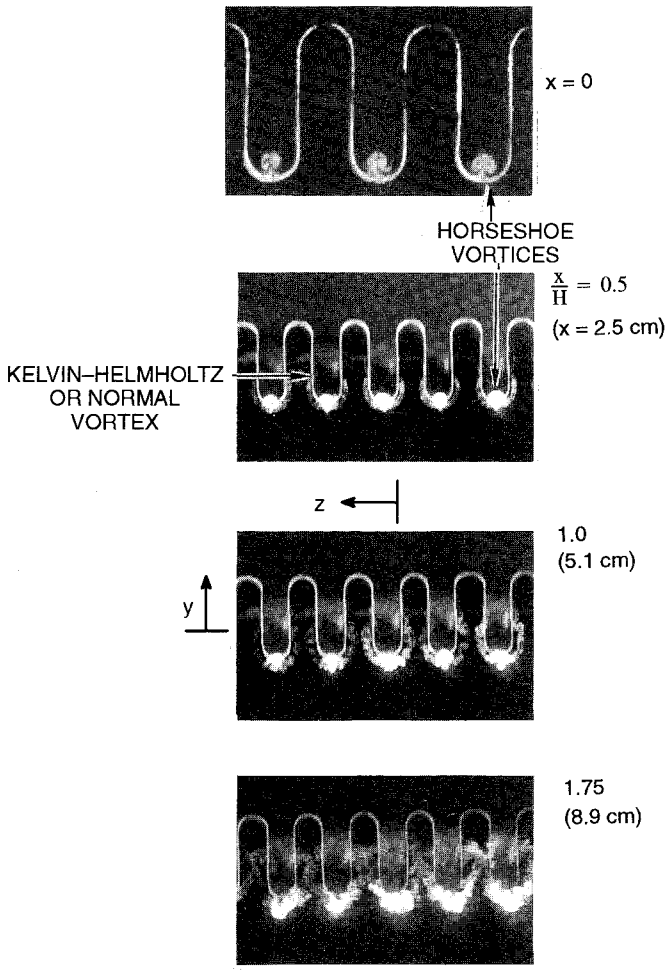

Fig. 6 Cross-stream laser sheet of lobed mixer free shear layer.

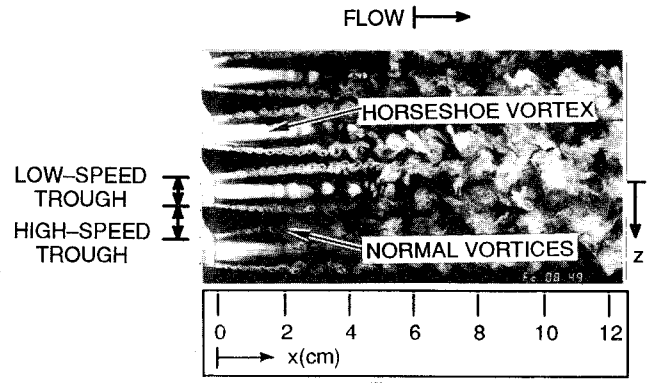

Fig. 7 Horizontal laser sheet of lobed mixer free shear layer.

Lobed-Mixer Free Shear Layer

The majority of the data presented here is for the laminar case since, surprisingly, the turbulent case was found to be very similar (unlike the planar free shear layer). Figure 3 defines the nomenclature used to describe areas of the lobe-mixer geometry (high-speed trough and peak, low-speed trough and peak).

Flow Visualization

The smoke injection technique used for the planar baseline case was applied to the lobed mixer to visualize the initial shear layer interface and downstream mixing region. However, somewhat different results were obtained. For the lobed mixer, the smoke migrated completely into the low-speed troughs as shown schematically in Fig. 3, limiting the initial interface visualization to a relatively small region. This migration of the viscous flow into the lobe troughs (thus thickening the trough boundary layer and thinning peak and vertical-edge boundary layers) is well documented by Skebe et al.[20] Flow visualization for two streamwise laser sheet positions (xy planes) are presented which are identified in Fig. 3 as the low-speed trough sheet and vertical-edge sheet.

Streamwise flow visualization of the lobed mixer (laminar initial conditions) is shown in Fig. 5. The low-speed trough view (Fig. 5a) clearly shows a vortex sheet due to the Kelvin-Helmholtz instability. The vortex sheet becomes turbulent and exhibits an increasing wavelength (due to vortex pairing) much like the planar case. Because of the thickened trough boundary layer, weak, opposite-sign vorticity is also observed on the upper edge of the smoke starting at x = 3 cm. The vertical-edge view (Fig. 5b) shows the Kelvin-Helmholtz vortices shedding from the vertical edge of the lobed mixer (which are connected to the vortices shown in the low-speed trough view). The vortices are inclined to the axial direction, perpendicular to the flow emanating from the high-speed trough at the lobe angle of ε = 15 deg. This vortex preference indicates that the high-speed flow dominates the shear layer structure (as is well documented in the planar case). Note also, the initial vertical spreading rate of the smoke due to the cross-stream flow is at the lobe angle ε = 15 deg (Fig. 5b). The flow structure observed in Fig. 5 is consistent with the results of Manning[9] who studied the molecular mixing in a two-stream, mixing-duct experiment (using the visible reaction of phenolphthalein and sodium hydroxide solution in water to visualize the Kelvin-Helmholtz vortex structure). Manning termed this vortex structure the normal (to the stream) vorticity; the same terminology will be used here.

Attempts to inject smoke into the high-speed flow usually tripped the boundary layer, which in turn masked the flow structure. One marginally successful method (shown in Ref. 12) confirmed that normal vortices were shedding from the high-speed

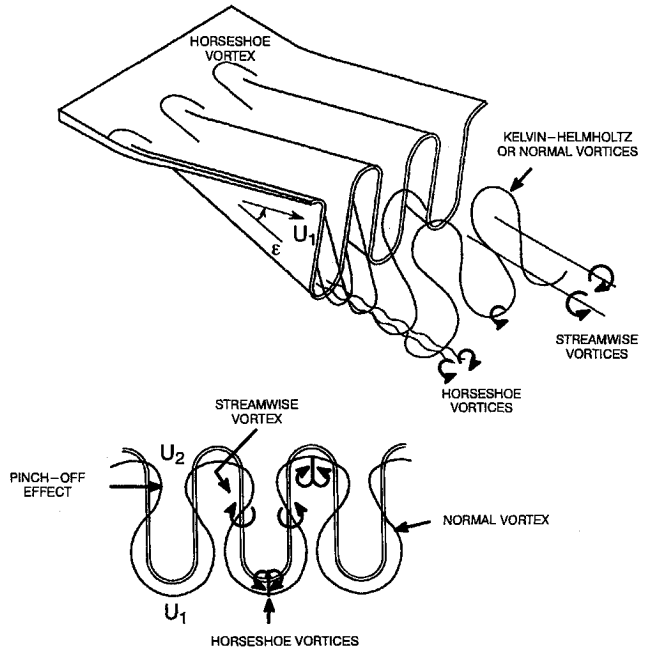

Fig. 8 Schematic of lobed mixer free shear layer vortical structure.

trough indicating that the normal vortex filaments were continuously connected across the convoluted trailing edge.

The cross-stream visualization (yz plane) at the exit plane, shown in Fig. 6, reveals a counter-rotating vortex pair in each low-speed trough. Each counter-rotating pair represents the legs from adjacent horseshoe vortex structures that are wrapped around the lobed peaks. The same pattern exists in the high-speed troughs, though is not visualized for reasons noted earlier. Though the horseshoe vortex structures have been suggested in previous studies (for example, Ref. 7), this result is the best known visualization and provides unquestionable evidence of their existence. The observed frame-to-frame steadiness of the horseshoe vortices indicates that the boundary-layer development through the lobed mixer remained laminar.

Figure 6 also documents three other cross-stream planes, showing the interaction of the streamwise vorticity with the normal vortex. The streamwise vorticity causes the normal vortex to deform such that it is bulged at the troughs thus pinching off the normal vortex between troughs. The horizontal laser sheet (Fig. 3) shown in Fig. 7 cuts through the vertically oriented segments of the normal vortices and grazes the horseshoe vortices. The normal vortex sheets are seen to migrate toward the vortex sheets of neighboring low-speed troughs (due to the deformation by the steamwise vorticity). The photograph shows that the small-scale turbulence begins to appear at $x = 4$ cm (compared to $x = 24$ cm for the planar case) and should correspond to enhanced molecular mixing. Also, note that the horseshoe vortices appear to breakup by $x = 4$ cm.

Based on the flow visualization, a schematic of the vortical structures is given in Fig. 8. The Kelvin-Helmholtz or normal vortex sheds from the convoluted trailing edge at an angle skewed relative to the lobed-mixer exit plane (but perpendicular to the high-speed trough flow that has been turned to the lobe angle, $\varepsilon = 15$ deg). The legs of the horseshoe vortices that ride on top of the normal vortices presumably get strained and amplified on the braids of the normal vortices. As a result of the streamwise vorticity, the normal vortices are bulged at the lobe troughs and eventually pinch off with adjacent vertical segments. Also, the normal vortex from the high-speed trough is biased toward the centerline when compared to the normal vortex from the low-speed trough due to the boundary layer thickening and thinning through the lobed mixer and the relative position of the high-speed flow (see Ref. 12 for explanation). At the vortex pinch-off location ($x \approx 8$ cm), the turbulence appears to become more intense (see Fig. 6, $x/H = 1.75$) suggesting the vortex merging process is an unstable interaction.

It is important to note that the scale of the normal vorticity is much smaller than that of the planar case. The initial wavelength is about $\lambda_{kh} = 6$ mm (see Fig. 5), one-fourth the initial value of the planar case (see Fig. 4). This scale reduction is due to the boundary-layer thinning that occurs along the high-speed peaks and vertical edges. Thus, the lobed mixer introduces a smaller scale into the flow earlier and, thus, should enhance the mixing at the molecular scale.

Mean Velocity Results

The development of the mean axial velocity for the lobed mixer (laminar) is shown on the left of Fig. 9 in terms of gray scales and contours. Consistent with the flow visualization, the low-speed trough flow is observed to penetrate farther than the high-speed flow. The contours are seen to be pinched off above and below the centerline between troughs due to cross-stream convection of the streamwise vorticity, analogous to the deformation of the normal vortices. From $x/H = 3$ to 9, the high-speed and low-speed flows bounded approximately by the normal vorticity are rapidly mixed to a uniform value of $U/\Delta U \approx 1.7$. This rapid mixing of flows is believed to be due to the introduction of the intense small-scale vorticity and turbulence over a large region of the flow. From $x/H = 9$ to 24 (see Ref. 12 for $x > 12H$), the high-speed flow is observed to slowly mix vertically into this plateau-like region of the velocity at a more conventional shear layer spreading rate.

Streamwise Vorticity

Contours of streamwise vorticity given in the middle of Fig. 9 (calculated from the mean cross-stream velocity components) show that the initial vorticity at $x/H = 1.75$, as expected, displays alternating positive and negative vorticity aligned with the vertical lobe edges. The figure also indicates that the streamwise vorticity introduced by the lobed mixer is largely dissipated downstream of $x/H = 6$, presumably due to the intense small-scale mixing of the normal vorticity and turbulent cascading of energy.

Another way to quantify the streamwise vorticity is by evaluating the streamwise circulation (line integral of velocity around a rectangle which encompasses one-half the lobe wavelength, as indicated in Fig. 10). This calculation was performed over six cells of measured data with the absolute magnitudes of the calculated circulation then averaged. The results of these computations are shown in Fig. 10 and verify the rapid decrease of streamwise vorticity with axial distance. The laminar and turbulent data are seen to be nearly identical. The initial value at $x/H = 0$ is from the theoretical model developed by Skebe et al.,[20] which when extended to the shear layer case[12] give an exit plane circulation of

$$\frac{\Gamma}{(\bar{U}H \tan \varepsilon)} = 4 \tag{1}$$

This theoretical value appears to be consistent with the calculated values obtained from the measurements, confirming the model validity.

Fluctuating Velocity Results

The right side of Fig. 9 presents the turbulent kinetic energy k (Ref. 12 presents the three Reynolds shear stresses). At $x/H = 1.75$, the turbulent kinetic energy shows a very intense turbulence pattern consistent with the pinched-off, normal vortex pattern. The peak values are comparable to the peak values of the laminar-planar case, but are more widely spread in the lobed-mixer case and occur much farther upstream. Where the normal vortices have merged at the pinch-off location ($x/H = 1.75$ between troughs), there is an increased turbulence production suggesting an instability in the vortex merging process. The influence of the horseshoe vortex on the turbulence pattern appears to be negligible. Between $x/H = 1.75$ and 6, the turbulent kinetic energy distribution is seen to rapidly homogenize and then develop into a double-banded region for $x/H \geq 9$ with constant peak turbulent kinetic energy (see Ref. 12 for $x > 12H$).

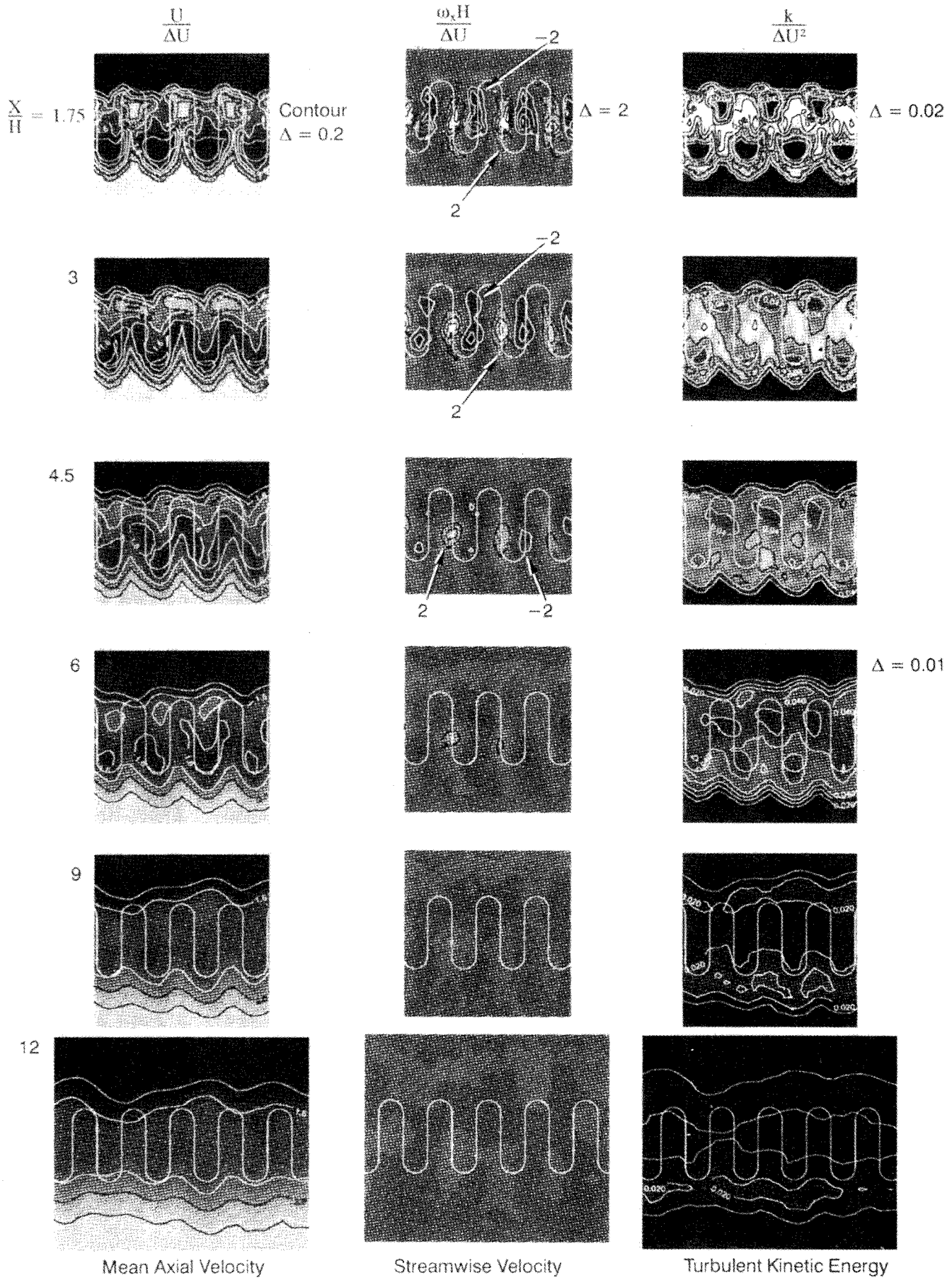

Fig. 9 Velocity measurements.

The double-banded structure is due to the axial velocity plateau, discussed earlier, which results in a two-layered shear layer. Note that the peak values in the double-banded region are about 2.5 times smaller than the far-field values for the baseline planar case (see Ref. 12). The lower values of the lobed-mixer case are due to the two weaker (lower velocity ratio) shear layers of the two-layered flow (note that far-field turbulence level of a shear layer scales with the square of the velocity difference).

Shear Layer Growth

Figure 11 gives the shear layer growth in terms of the momentum thickness

$$\theta = \int \frac{(U-U_2)(U_1-U)}{\Delta U^2}\, dy \qquad (2)$$

which is a measure of the momentum entrained into the shear layer. The circular symbols in the figure correspond to the lobed-mixer case and the square symbols correspond to the baseline planar case. Both laminar (open symbols) and turbulent data (closed symbols) are given for both cases. Each data point represents the spanwise average of the momentum thickness.

The turbulent planar data grows linearly over most of the shear layer development. The linear growth behavior is consistent with classical thin-layer approximations assuming simple eddy-viscosity turbulent transport.[21] The laminar planar case achieves this linear behavior for $x/H \geq 12$ ($x = 61$ cm). Initially the laminar growth is very small, followed by a region of more rapid nonlinear growth, and finally followed by the region of linear growth when the small-scale turbulence is well established and gradient-type transport dominates. The far-field growth rate for the laminar case, consistent with a previous investigation,[22] is observed to be about 20% greater than the turbulent case.

For the lobed mixer, the growth rate is independent of the initial conditions (unlike the planar case). The growth rate is very rapid for the first six lobe height ($x/H \leq 6$), with growth rates less than the planar cases farther downstream. Thus, the region of maximum effectiveness for the lobed mixer is the first six lobe heights (at least for this velocity ratio). This result is consistent with both the flow visualization and the velocity measurements discussed previously (which show there is coherent streamwise and normal vorticity in this region). Downstream of $6H$, the coherent vorticity is dissipated and momentum transport occurs via more conventional gradient-type turbulent mechanisms. The growth rate in this region is below that of the planar cases consistent with the reduced turbulence intensity of the two-layered shear layer for the lobed-mixer far field.

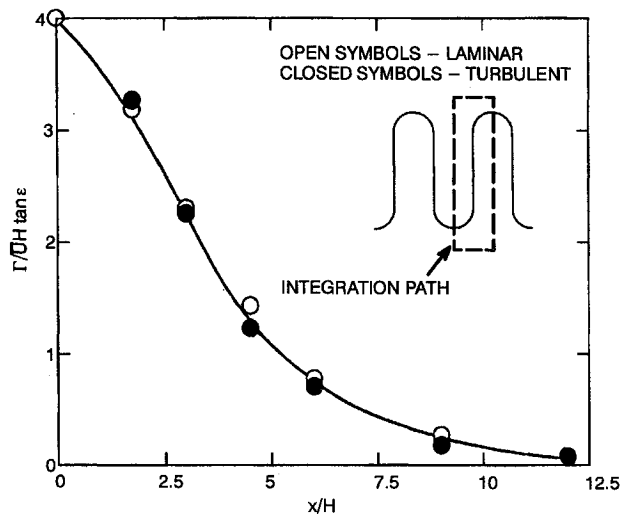

Fig. 10 Streamwise circulation development.

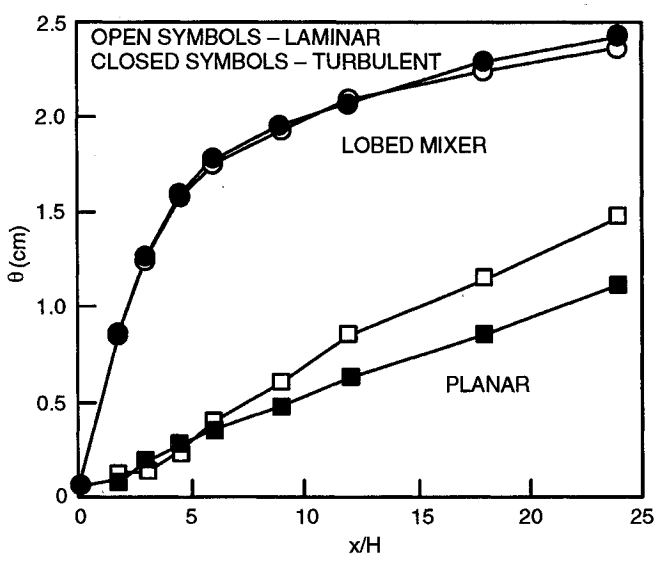

Fig. 11 Momentum thickness development.

Effect of Turbulent Boundary Layers

As seen in the circulation development and shear layer growth, the lobed-mixer shear layer is relatively insensitive to the initial boundary-layer condition (laminar vs turbulent). As reported in detail in Ref. 12, the flow visualization clearly showed that the normal vortex structure is still present for turbulent initial conditions. In terms of the velocity data, the turbulent data were very similar in magnitude and structure to the laminar case except that the contour patterns were more regular and symmetric. The irregularity of the laminar case is believed to be analogous to the undulations observed for the laminar planar shear layer due to the streamwise instability. The similarity of the laminar initial conditions is due to the small-scale vorticity caused by the boundary-layer thinning over the lobed mixer and subsequent early turbulent transition.

Lobed-Mixer Applications

The significance of the current results to lobed-mixer applications, such as the mixer ejector, is primarily the limited range of enhanced mixing that was found to occur downstream of a lobed mixer. The present results indicate an axial distance of $6H$ as the region of enhanced mixing. This criterion should be used to determine the axial length of the mixing region for a given application to insure optimal use of the mixer. The "natural" small-scale structure that occurs downstream of a mixer may be exploited for enhanced molecular mixing applications. Relative to a high-speed situation, such as the high-speed civil transport exhaust system, there exists significant evidence that the Kelvin-Helmholtz instability exists for compressible shear conditions. Hence, it is believed that the mixing mechanisms described herein are also present, to some degree, in high-speed applications.

Conclusions

A comprehensive experimental investigation of the vortical and turbulent structure in a free shear layer downstream of a lobed mixer has been conducted. The main result of this investigation is a new vortex structure has been confirmed to exist for the lobed mixer in addition to the well-known streamwise vortex array. This normal vortex (due to the Kelvin-Helmholtz instability) sheds periodically from the convoluted trailing edge of the lobed mixer and plays a major part in the enhanced mixing process (in combination with the streamwise vorticity). Thus, a velocity difference between the coflowing streams is an important feature for maximum mixing enhancement. The streamwise vorticity deforms the normal vortex into a pinched-off structure that is unstable and creates intense turbulence. The scale of the normal vortex for the lobed mixer is one-fourth that of the planar case (due to boundary-layer thinning on the high-speed side), thereby introducing much earlier

a small-scale turbulence over a large cross-stream area of the flow. In this manner, the lobed mixer provides enhanced mixing down to the molecular scale. The mixer shear layer growth for the first six lobe heights is substantially greater than the planar free shear layer (due to the normal and streamwise vortex interaction). Downstream of six lobe heights, the mixer growth rate slows considerably to a rate below that of the planar configuration due to the reduced turbulent kinetic energy of the doubled-layered shear layer and the completely dissipated streamwise and normal vorticities. Another important result is the effect of laminar vs turbulent initial boundary-layer conditions which was found to be negligible.

Acknowledgments

This study was funded by United Technologies Research Center. The support and guidance by Robert W. Paterson and William P. Patrick are gratefully acknowledged.

References

[1]Crouch, R. W., Coughlin, C. L., and Paynter, G. C.,"Nozzle Exit Flow Profile Shaping for Jet Noise Reduction," *Journal of Aircraft*, Vol. 14, No. 9, 1977, pp. 860–867.

[2]Kozlowski, H., and Kraft, G., "Experimental Evaluation of Exhaust Mixers for an Energy Efficient Engine," AIAA Paper 80-0188, June 1980.

[3]Presz, W. M., Morin, B. L., and Gousy, R. G., "Forced Mixer Lobes in Ejector Designs," *Journal of Propulsion and Power*, Vol. 4, No. 4, 1988, pp. 350–355.

[4]Lord, W. K., Jones, C. W., Stern, A. M., Head, V. L., and Krejsa, E. A., "Mixer Ejector Nozzle for Jet Noise Suppression," AIAA Paper 90-1909, July 1990.

[5]Presz, W. M., "Mixer/Ejector Noise Suppressors," AIAA Paper 91-2243, June 1991.

[6]Paynter, G. C., Birch, S. C., Spalding, D. B., and Tatchell, D. G., "An Experimental and Numerical Study of the 3-D Mixing Flows of a Turbofan Engine Exhaust System," AIAA Paper 77-204, Jan. 1977.

[7]Paterson, R. W., "Turbofan Mixer Nozzle Flow Field-A Benchmark Experimental Study," *Journal of Engineering for Gas Turbines and Power*, Vol. 106, July 1984, pp. 692–698.

[8]Povinelli, L. A., Anderson, B. H., and Gerstenmaier, W., "Computation of Three-Dimensional Flow in Turbofan Mixers and Comparison with Experimental Data," AIAA Paper 80-0227, Jan. 1980.

[9]Manning, T. A., "Experimental Studies of Mixing Flows with Streamwise Vorticity," M.S. Thesis, Massachusetts Inst. of Technology, Cambridge, MA, Sept. 1991.

[10]Elliott, J. K., Manning, T. A., Qiu, Y. J., Greitzer, E. M., Tan, C. S., and Tillman, T. G., "Computational and Experimental Studies of Flow in Multi-Lobed Forced Mixers," AIAA Paper 92-3568, July 1992.

[11]Eckerle, W. A., Sheibani, H., and Awad, J., "Experimental Measurements of Vortex Development Downstream of a Lobed Forced Mixer," *Journal of Engineering for Gas Turbines and Power*, Vol. 114, Jan. 1992, pp. 63–71.

[12]McCormick, D. C., "Vortical and Turbulent Structure of Planar and Lobed Mixer Free-Shear Layers," Ph.D. Dissertation, Dept. of Mechanical Engineering, Univ. of Connecticut, Storrs, CT, May 1992.

[13]Blair, M. F., Bailey, D. A., and Schlinker, R. H., "Development of a Large-Scale Wind Tunnel for the Simulation of Turbomachinery Airfoil Boundary Layers," *Journal of Engineering for Power*, Vol. 103, Oct. 1981, pp. 678–687.

[14]White, F. M., *Viscous Fluid Flow*, McGraw-Hill, New York, 1974, p. 404.

[15]Hama, F. R., "An Efficient Tripping Device," *Journal of the Aeronautical Sciences*, Vol. 24, March 1957, pp. 236, 237.

[16]Lekakis, I. C., Adrian, R. J., and Jones, B. G., "Measurement of Velocity Vectors with Orthogonal and Non-orthogonal Triple-Sensor Probes," *Experiments in Fluids*, Vol. 7, Feb. 1989, pp. 228–240.

[17]Michalke, A., "On Spatially Growing Disturbances in an Inviscid Shear Layer," *Journal of Fluid Mechanics*, Vol. 23, Pt. 3, Nov. 1965, pp. 521–544.

[18]Lasheras, J. C., Cho, J. S., and Maxworthy, T., "On the Origin and Evolution of Streamwise Vortical Structures in a Plane, Free Shear Layer," *Journal of Fluid Mechanics*, Vol. 172, Nov. 1986, pp. 499–525.

[19]Ho, C. M., and Huang, L. S., "Subharmonics and Vortex Merging in Mixing Layers," *Journal of Fluid Mechanics*, Vol. 119, June 1982, pp. 443–473.

[20]Skebe, S. A., Paterson, R. W., and Barber, T. J., "Experimental Investigation of Three-Dimensional Forced Mixer Lobe Flow Fields," AIAA Paper 88-3785, July 1988, pp. 1999–2006.

[21]Tennekes, H., and Lumley, J. L., "A First Course in Turbulence," MIT Press, Cambridge, MA, 1972, pp. 127–130.

[22]Bell, J. H., and Mehta, R. D., "Development of a Two-Stream Mixing Layer from Tripped and Untripped Boundary Layers," *AIAA Journal*, Vol. 28, No. 12, Dec. 1990, pp. 2034–2042.